

## The effects of stellar activity on optical high-resolution exoplanet transmission spectra

P. WILSON CAULEY,<sup>1</sup> CHRISTOPH KUCKEIN,<sup>2</sup> SETH REDFIELD,<sup>3</sup> EVGENYA L. SHKOLNIK,<sup>1</sup> CARSTEN DENKER,<sup>2</sup> JOE LLAMA,<sup>4</sup>  
AND MEETU VERMA<sup>2</sup>

<sup>1</sup>Arizona State University, School of Earth and Space Exploration, Tempe, AZ 85287

<sup>2</sup>Leibniz-Institut für Astrophysik Potsdam (AIP), An der Sternwarte 16, 14482 Potsdam, Germany

<sup>3</sup>Wesleyan University, Astronomy Department, Van Vleck Observatory, Middletown, CT

<sup>4</sup>Lowell Observatory, Flagstaff, AZ 86001

(Received 2018 June 4; Accepted 2018 August 28)

Submitted to AJ

### ABSTRACT

Chromospherically sensitive atomic lines display different spectra in stellar active regions, spots, and the photosphere, raising the possibility that exoplanet transmission spectra are contaminated by the contrast between various portions of the stellar disk. To explore this effect, we performed transit simulations of G and K-type stars for the spectral lines Ca II K at 3933 Å, Na I 5890 Å, H I 6563 Å (H $\alpha$ ), and He I 10830 Å. We find that strong facular emission and large coverage fractions can contribute a non-negligible amount to transmission spectra, especially for H $\alpha$ , Ca II K, and Na I D, while spots and filaments are comparatively unimportant. The amount of contamination depends strongly on the location of the active regions and the intrinsic emission strength. In particular, active regions must be concentrated along the transit chord in order to produce a consistent in-transit signal. Mean absorption signatures in Na I and H $\alpha$  for example, can reach  $\approx 0.2\%$  and  $0.3\%$ , respectively, for transits of active latitudes with line emission similar in strength to moderate solar flares. Transmission spectra of planets transiting active stars, such as HD 189733, are likely contaminated by the contrast effect, although the tight constraints on active region geometry and emission strength make it unlikely that consistent in-transit signatures are due entirely to the contrast effect. He I 10830 Å is not strongly affected and absorption signatures are likely diluted, rather than enhanced, by stellar activity. He I 10830 Å should thus be considered a priority for probing extended atmospheres, even in the case of active stars.

### 1. INTRODUCTION

Transmission spectroscopy has been the workhorse for measuring the physical properties of exoplanet atmospheres, probing from the deep molecular layers of hot planets (Sing et al. 2016) out to the thermosphere (Redfield et al. 2008; Wyttenbach et al. 2015) and beyond to the unbound exosphere (Vidal-Madjar et al. 2003; Ehrenreich et al. 2015). These observations have revealed a variety of molecular (e.g., Knutson et al. 2007; Snellen et al. 2010; Deming et al. 2013; Kreidberg et al. 2015; Brogi et al. 2016) and atomic species in exoplanet atmospheres (e.g., Jensen et al. 2011; Pont et al. 2013; Cauley et al. 2015; Wilson et al. 2015; Wyttenbach et al. 2017; Casasayas-Barris et al. 2017; Spake et al. 2018), detailed the presence of cloud layers (Kreidberg et al. 2014), and even probed the dynamics of bound and unbound material (Bourrier et al. 2015; Louden & Wheat-

ley 2015; Brogi et al. 2016). The *James Webb Space Telescope* and upcoming extremely large ground-based telescopes will greatly expand the sample of planetary atmospheres that can be recorded in transmission.

Exoplanet transmission spectra are always contaminated by star spots and faculae to some degree: the stellar disk is heterogeneous and the weighting of the integrated in-transit signal towards the unocculted regions of the stellar disk can produce spurious features in the transmission spectrum (Berta et al. 2011; Sing et al. 2011; Cauley et al. 2017a; Rackham et al. 2018). We hereon refer to this phenomenon as the *contrast effect* due to its origin in the stark differences between the spectra of various active region features. Time-variable levels of stellar activity, as opposed to the effects induced on the observed spectrum by the planet's shadow, can also impact transmission spectra created by combining data from different epochs (Zellem et al. 2017). While more attention has recently been paid to the magnitude of the contrast effect, which, for example, has been used to estimate faculae coverage for GJ 1214 (Rackham et

al. 2017) and possible contamination of H $\alpha$  transmission spectra for HD 189733 b (Cauley et al. 2017a), a more complete understanding is needed of the magnitude of contrast contamination in exoplanet transmission spectra.

Progress on this front has been made by Rackham et al. (2018), who showed how active regions and spots on M-dwarfs can affect the strength of molecular features in the transmission spectra of small rocky planets. For many faculae and spot configurations, important molecular features, such as O<sub>2</sub>, H<sub>2</sub>O, and CO<sub>2</sub>, can be contaminated at the level of  $\approx 10 - 30\%$ . These results highlight the need for stronger constraints on facular and spot coverage fractions in order to interpret transmission spectra of transiting planets around M-dwarfs.

While molecular features such as H<sub>2</sub>O and CO are observed at pressures of  $\approx 1$  bar in exoplanet atmospheres (e.g., Kreidberg et al. 2015), the cores of atomic lines such as Na I D, H $\alpha$ , and He I 10830 Å sample pressures of  $\approx 1$   $\mu$ bar at higher altitudes (Huang et al. 2017; Oklopčić & Hirata 2018). Atomic transitions were the first detections in exoplanet atmospheres (Charbonneau et al. 2002; Redfield et al. 2008; Snellen et al. 2008) and continue to be important diagnostics of the thermosphere (e.g., Cauley et al. 2016; Barnes et al. 2016; Cauley et al. 2017a,b; Chen et al. 2017; Khalafinejad et al. 2017; Wyttenbach et al. 2017; Casasayas-Barris et al. 2017). Recently, Spake et al. (2018) reported the first detection of helium in the extended atmosphere of WASP-107 b, confirming the potential of the He I 10830 Å line as a probe of hot planet exospheres, as suggested by early theoretical studies in atmospheric characterization (Seager & Sasselov 2000). High-resolution observations of atomic lines can also provide information on velocity flows in the atmosphere (e.g., Wyttenbach et al. 2015; Louden & Wheatley 2015; Cauley et al. 2017a) and cross-correlation analysis of high-resolution molecular absorption can yield constraints on planetary rotation (Snellen et al. 2010, 2014; Brogi et al. 2016). If non-negligible for hot Jupiter systems, the contrast effect can contaminate the magnitude of the measured absorption and may bias cross-correlation signatures towards active region features.

In this paper we explore the effect of faculae and spots on the strength of observed atomic absorption features in exoplanet transmission spectra. We focus on G and K stars and spectral lines which have a significant contribution from the chromosphere, specifically the transitions of Ca II K at 3933 Å, the Na I 5896 Å component of the Na I D doublet, H I 6563 Å (H $\alpha$ ), and He I 10830 Å. The details of the simulations are outlined in Section 2 and the model results are given in Section 3. Included in Section 3 is a transit of the resolved solar disk in order to provide some context for the rest of the simulation parameters. A discussion of how the results compare with observations is presented in Section 4 and a brief summary of our conclusions is given in Section 5.

## 2. SIMULATIONS OF ACTIVE STELLAR SURFACE TRANSITS

Our approach to simulating planetary transits of active stellar surfaces is similar to the procedure described in Cauley et al. (2017a). Each simulation samples the integrated stellar spectrum at ten different points across the planet’s transit. The mean in-transit spectrum changes negligibly if the number of sampled transit points is increased beyond ten. The in-transit spectrum is then divided by the integrated out-of-transit spectrum to produce the contrast spectrum, which we label  $S_{\text{in}}/S_{\text{out}}$ .  $S_{\text{in}}/S_{\text{out}}$  varies depending on which portion of the stellar disk is occulted by the planet. We note that the weaker doublet members Ca II H and Na I 5896 Å are not shown here but, due to their lower oscillator strengths, their contrast signals are constrained to be lower than those for Ca II K and Na I 5890 Å. The integrated model spectra are convolved with a Gaussian kernel to a resolving power of  $R \approx 70,000$  to approximate a typical high-resolution optical spectrograph.

We explore four different effective temperatures,  $T_{\text{eff}} = 4500, 5000, 5500,$  and  $6000$  K, with  $\log g = 4.5$  and  $[\text{Fe}/\text{H}] = 0.0$ , which covers mid-K to early G-type main sequence stars. Two different values, 0.01 and 0.02, of the ratio  $(R_p/R_*)^2$  are tested. These quantities cover a majority of the transit depths currently probed by high-resolution transmission spectroscopy. The stellar equatorial rotational velocity is set at  $2 \text{ km s}^{-1}$  for all cases, including the solar test case, and we assume rigid rotation. Although G and K stars shows a range of  $v \sin i$  values, the vast majority of transiting planet hosts with  $T_{\text{eff}} \leq 6000$  K have  $v \sin i \lesssim 6 \text{ km s}^{-1}$ . The exact value of the stellar rotational velocity contributes significantly less to the shape of the contrast spectrum compared with the active region parameters. For this reason a constant  $v \sin i$  is chosen for the sake of simplifying the parameter space. The transit impact parameter is set at  $b = 0.5$  for all simulations. The stellar disk has a spatial resolution of  $0.0025 R_*$ , resulting in an  $800 \times 800$  Cartesian grid. The planet is simulated in an aligned prograde orbit in all cases.

The model spectra are generated using SPECTRUM (Gray & Corbally 1994). We calculate the spectra at twenty four different values of  $\mu = \cos \theta$ , where  $\theta$  is the angle between the normal vector to the stellar surface and the line of sight, from  $\mu = 0.01 - 1.0$ . We then interpolate the ratio of the spectra at each wavelength onto a  $\mu$ -grid representing the stellar disk, resulting in a cube of  $I(\mu)/I(\mu = 1)$  as a function of wavelength.

Accounting for the wavelength dependence of limb darkening across a single spectral line is critical: center-to-limb variations, or CLVs, are non-negligible for strong photospheric lines and can mimic planetary atmospheric absorption (Yan et al. 2015; Czesla et al. 2015; Khalafinejad et al. 2017; Cauley et al. 2017a; Yan et al. 2017). Examples of the intensity ratios for each line are

shown in Figure 1 for  $T_{\text{eff}} = 5500$  K. Note that CLVs are a function of  $T_{\text{eff}}$  so the curves in Figure 1 will change with different  $T_{\text{eff}}$ .

The Ca II K curves behave differently than Na I D and H $\alpha$ : the line core has a steeper limb-darkening function than the wing, although the effect is small. This is also contrary to the solar observations of White & Suemoto (1968) and Ermolli et al. (2010). Both White & Suemoto (1968) and Ermolli et al. (2010), however, measure the wing limb-darkening at  $\approx \pm 4$  Å from line center, whereas we show the  $\pm 1$  Å case. The Ca II K line is much broader than Na I D and H $\alpha$  for the  $T_{\text{eff}}$  values we examine and thus the  $\pm 1$  Å case samples a steeper portion of the line wing. The discrepancy between our simulations and the observed solar case can likely be attributed to such differences.

One important caveat regarding the CLVs calculated here is that SPECTRUM is an LTE code. The cores of strong lines, such as H $\alpha$ , Na I D, and Ca II K, in main sequence G and K stars are formed high up in the stellar photosphere, near the base of the chromosphere, where LTE is no longer valid. Including non-LTE effects would produce more accurate CLV curves and line profiles. However, as we will show, the dominant effects in our simulations are the active region emission and coverage fraction parameters. Thus any changes to the exact CLV values by including non-LTE spectral synthesis will be small (see Figure 11 of Yan et al. 2017) compared with the effects of stellar active regions.

To make the simulations more computationally efficient, we do not calculate a model spectrum at every  $\mu$  value from disk center to the limb. Instead, we use the derived limb darkening law to adjust the  $\mu = 1.0$  spectrum at each disk position before that specific grid cell is added to the disk-integrated spectrum.

The facular contrast exhibits limb brightening relative to the underlying photosphere, which is the result of the increased projected emitting area of these optically thin features as the line-of-sight moves closer to the stellar limb (Berger et al. 2007). This brightening is a function of wavelength, with bluer wavelengths exhibiting larger effects. We adopt the solar limb brightening law of Gondoin (2008) (their equation 5). While this treatment is not strictly valid out to  $\approx 10830$  Å, where the average contrast is approximately equal to the bolometric value, the influence on the simulations is much smaller than other factors, e.g., the strength of the facular emission. We also tested the limb brightening scaling from Meunier et al. (2010), which is appropriate for wavelengths between 4700 Å and 5500 Å, and found negligible differences ( $\lesssim 10\%$ ) to the Gondoin (2008) scaling. Note that the facular scaling is applied in addition to line core emission, i.e., even at disc-center where the facular temperature difference is zero these is still line emission.

Facular limb brightening is a function of spectral type and magnetic field strength (e.g., Beek et al. 2015). Thus a more precise approach would include these ef-

fects by deriving brightening laws for individual spectral lines via simulation. Accounting for such effects is beyond the scope of this paper and is likely unnecessary given the relatively small contribution of facular brightening to the in-transit contrast spectra. Facular contrast temperatures are fairly similar to the photospheric temperature for the Sun (Unruh et al. 1999). For this reason, and because  $a_{\text{act}}$  and  $f_{\text{act}}$  are the more critical parameters, we fix the facular contrast temperature at  $\Delta T_{\text{fac}} = 50$  K. The facular<sup>1</sup> spectra are limb brightened before being added to the underlying photospheric spectrum, which is limb darkened.

To simulate transits of active stellar surfaces, we consider the effects of facular regions, spots, and the photosphere. We do not include filaments here since our previous work found them to be unimportant relative to spots and faculae (Cauley et al. 2017a). All spots and faculae are assumed to be circular and facular regions are allowed to overlap to create more complicated shapes. The radius of individual facular features ranges from a minimum of three grid pixels, or 0.002% of the stellar disk area, up to  $\approx 10$  grid pixels. Although faculae on the Sun can have sizes as small as a few hundred kilometers (e.g., Title et al. 1992; Viticchié et al. 2011), or  $\approx 10^{-7}$  of the solar disk, the value of  $(R_p/R_*)^2$  and the total facular coverage fraction, combined with their positions on the disk, are much stronger contributors to the in-transit contrast effect. We thus do not consider smaller facular sizes, as this only serves to add computational time to the simulations. Features are placed randomly on the stellar disk with constraints provided for different scenarios, e.g., active belts centered at a specific latitude. Active regions and spots near the limb are foreshortened.

We use the same model stellar spectra for the spots and photosphere, e.g., for a star with  $T_{\text{eff}} = 5500$  K and a spot temperature difference of 500 K, a  $T_{\text{eff}} = 5000$  K model spectrum is selected for the spot. The relative flux of the spot spectrum is scaled by the ratio of the model continuum intensities of the  $\mu = 1.0$  (disk-center) spectra. For Ca II K and He I 10830 Å we add an additional component to the spot spectrum: an emission line for Ca II K and an absorption line for He I 10830 Å (see Figure 2). We fix the maximum emission value to 0.2 and the minimum absorption to 0.8 for Ca II K and He I 10830 Å, respectively. The spot spectra are limb darkened using the derived values for the appropriate spot temperature.

The facular spectra are constructed by adding or subtracting a Gaussian to the underlying photospheric spectrum depending on which line is being tested. The strength of the intrinsic active region emission is de-

<sup>1</sup> We will use faculae to refer to all bright active regions on the stellar surface and ignore the differences between faculae, plage, and magnetic bright points.

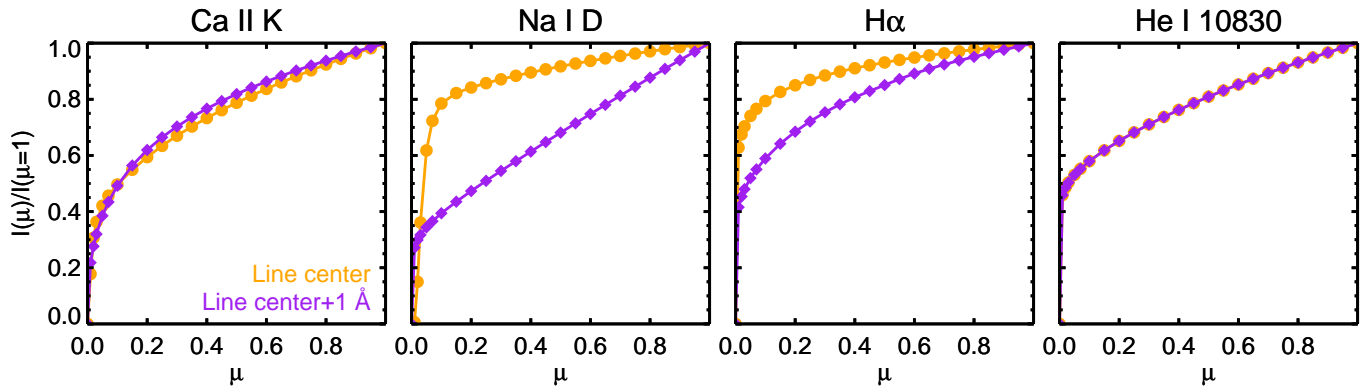


**Figure 1.** Normalized center-to-limb variations for  $T_{\text{eff}} = 5500$  K. The line core is shown in orange and a  $+1 \text{ \AA}$  offset from line center is shown in purple. Note that the line cores of Na I and  $H\alpha$  tend to show less steep  $I(\mu)$  functions compared with the line wing and continuum. He I 10830 is not present in the photosphere of a 5500 K star and thus shows no difference between the continuum at the two different wavelengths. These curves change as a function of  $T_{\text{eff}}$  with Na I showing the most dramatic differences.

defined as  $a_{\text{act}}$  and is the ratio of the Gaussian emission line to the photospheric absorption line. Thus the same value of  $a_{\text{act}}$  for different lines can produce different levels of absolute flux depending on the depth of the photospheric absorption; the ratio of the lines, however, is the same for identical values of  $a_{\text{act}}$ . The FWHM of the Gaussian is fixed to  $20 \text{ km s}^{-1}$ , roughly the width of the transmission spectra observed in Cauley et al. (2015, 2016, 2017a). We do not attempt to reproduce the exact shape of the active region emission, e.g., the double-peaked Ca II K lines, since most observations cannot fully resolve these features.

The contrast, or  $a_{\text{act}}$  for our simulations, in bright active regions shows a strong dependence on magnetic field strength for the Sun, decreasing for field strengths up to  $\approx 50$  G and then monotonically increasing out to  $\approx 1000$  G where the dependence plateaus (Kahil et al. 2017). Thus stars will most likely exhibit active regions with varying levels of contrast across the disk. Since we are interested in the average effect of these features on a planetary transmission signature, we assume that all bright active regions have the same contrast. Letting  $a_{\text{act}}$  vary over the stellar disk could more strongly affect time series absorption values, which we do not present here.

Figure 2 demonstrates that He I 10830  $\text{\AA}$  shows absorption in active regions on the Sun. Andretta & Giampapa (1995) find that chromospheres  $\approx 100\times$  denser than the solar case can produce He I 10830  $\text{\AA}$  in emission. We do not simulate these high-density cases but we speculate that the results would be similar to the emission line cases ( $H\alpha$ , Na I D, and Ca II K) explored here. In the case of He I 10830  $\text{\AA}$ ,  $a_{\text{act}}$  refers to the depth of the Gaussian absorption feature below the continuum, which is set equal to 1.0 in all simulations.

Definitions and value ranges for the various parameters used in the simulations are given in Table 1. We are motivated to search across a broad parameter space in

order to explore the extent to which observed exoplanet transmission signals can be reproduced by the contrast effect. We find some guidance from the Sun (see Section 3.1). Figure 2 shows observed, spatially-resolved sunspot (top row) and facular (bottom row) spectra (see Section 3.1 for details). For example, in the Ca II H faculae panel in Figure 2,  $a_{\text{act}} \approx 1.0$ , for  $H\alpha$   $a_{\text{act}} \approx 0.6$ , and for Na I D  $a_{\text{act}} \approx 0.8$ . Thus we explore a range of  $a_{\text{act}}$  consistent with the solar case but which includes values that may be more indicative of more active stars, e.g.,  $a_{\text{act}}$  can be as high as 3.0 or 4.0 in M-class flares (Johns-Krull et al. 1997; Xu et al. 2016).

Spots are generally described as being composed of an inner umbral region and a surrounding penumbral annulus. The umbral region is cooler than the penumbra, showing a greater temperature differential with the surrounding photosphere. This average differential of both umbral and penumbral regions, or  $\Delta T_{\text{sp}}$ , depends on  $T_{\text{eff}}$ , with  $\Delta T_{\text{sp}}$  increasing with larger  $T_{\text{eff}}$  (see Figure 7 of Berdyugina 2005). According to Berdyugina (2005),  $\Delta T_{\text{sp}}$  varies from  $\approx 1000$  K for  $T_{\text{eff}} \approx 4500$  K up to  $\approx 1800$  K for  $T_{\text{eff}} \approx 5800$  K; there is little data for stars with  $T_{\text{eff}} \gtrsim 5800$  K. We do not differentiate between umbral and penumbral regions, which can have temperatures that differ by  $\approx 1000$  K and corresponding differences in the brightness of chromospheric line emission; the spot temperatures in the simulations are considered an average of the two. Thus we explore a different range of  $\Delta T_{\text{sp}}$  for each  $T_{\text{eff}}$ , varying from  $\Delta T_{\text{sp}} = 500$  K for  $T_{\text{eff}} = 4500$  K up to  $\Delta T_{\text{sp}} = 1500$  K for  $T_{\text{eff}} = 6000$  K.

Finally, spot and facular coverage fractions are chosen to simulate reasonable G and K-star values. Sunspot disk coverage fractions vary from  $\approx 0.001 - 0.010$  at solar minimum and maximum, respectively (Shapiro et al. 2014). Spot coverage fractions have been measured for active transiting exoplanet hosts: Morris et al. (2017) find a mean disk coverage fraction of  $3_{-1}^{+6}\%$  for HAT-P-11 b; Pont et al. (2013) determine an average spot

coverage fraction of  $\approx 1 - 2\%$  for HD 189733 b. Thus we conservatively explore values ranging from 0.3% up to the extreme case of 10%. For faculae, coverage fractions on the Sun vary between  $\approx 0.005$  and 0.04 (Shapiro et al. 2014). Plage coverage is similar, varying between  $\approx 0.002$  and 0.06 (Mandal et al. 2017). Combining the facular and plage coverages for the Sun, bright active regions can account for up to  $\approx 10\%$  of the solar disk. Estimating active region coverage fractions for main-sequence G and K stars other than the Sun is difficult. For this reason we extend our parameter exploration up to  $f_{\text{act}} = 50\%$  to account for the most active exoplanet hosts. We note that Andretta et al. (2017) find He I 10830 Å filling fractions as high as  $\approx 80\%$  for G and K-stars, although this is within the context of their specific chromospheric models.

### 3. SIMULATION RESULTS

Here we describe the results of the transit simulations for a variety of cases: transits of the resolved solar disk (Section 3.1), only star spots (Section 3.2), a uniform distribution of active regions (Section 3.3), transiting active latitudes (Section 3.4), and transiting slightly offset from active latitudes (Section 3.5). The solar disk transits are useful for comparisons to solar analogs with transiting hot planets and provide a realistic baseline example for the simulations. The spot-only case is unlikely to occur but is useful for demonstrating the contribution of spots to the contrast spectra. Finally, transits of simulated surfaces with different bright active region geometries cover the general (uniform active region distribution) and extreme (centered on active latitudes) cases for which the contrast effect is important.

#### 3.1. The Sun as a test case

The Sun is the only star for which we have high-resolution spectra at high spatial resolution of the stellar disk and thus provides a baseline example for realistic active region parameters in the spectral lines explored here. Most importantly, we are concerned with the *intrinsic* emission and absorption in spots and faculae. For stars with unresolved stellar surfaces, there is a degeneracy between the strength of the active region spectral feature and the coverage fraction of similar types of active regions (see Figure 17 of Cauley et al. 2017a). It is critical to break this degeneracy when considering the contrast effect for transiting planets. There is some evidence that the critical difference between active and less-active stellar spectra is the coverage fraction and not the intrinsic emission strength: Andretta et al. (2017) find a relatively narrow range of chromospheric densities are required to reproduce the equivalent width ratios of He I 5876 Å and He I 10830 Å for G and K-type stars exhibiting a large range of coverage fractions. More estimates of filling fractions for active stars are needed to confirm this behavior.

In order to provide some context for intrinsic active region features in our simulations, we have collected observed spectra of spots and facular regions on the Sun. These spectra are shown in Figure 2. The data are from a variety of sources. The sunspot umbra and quiet photosphere spectra in the upper row of Figure 2 are from the National Solar Observatory Solar Flux Atlas<sup>2</sup>. We normalize both the spot and quiet photosphere spectra to the continuum flux at  $\pm 7$  Å to emphasize the differences in the line core.

The plage and photosphere spectra for Na I and H $\alpha$  in the bottom row are from Kuckein et al. (2016). The faculae spectra are averages of  $5 \times 5$  pixel boxes of the brightest regions in sections 5 and 7 from their Figure 2. The quiet Sun photosphere spectrum is an average of all other pixels in sections 1 through 10, excluding the filament and bright regions selected for the facular spectra.

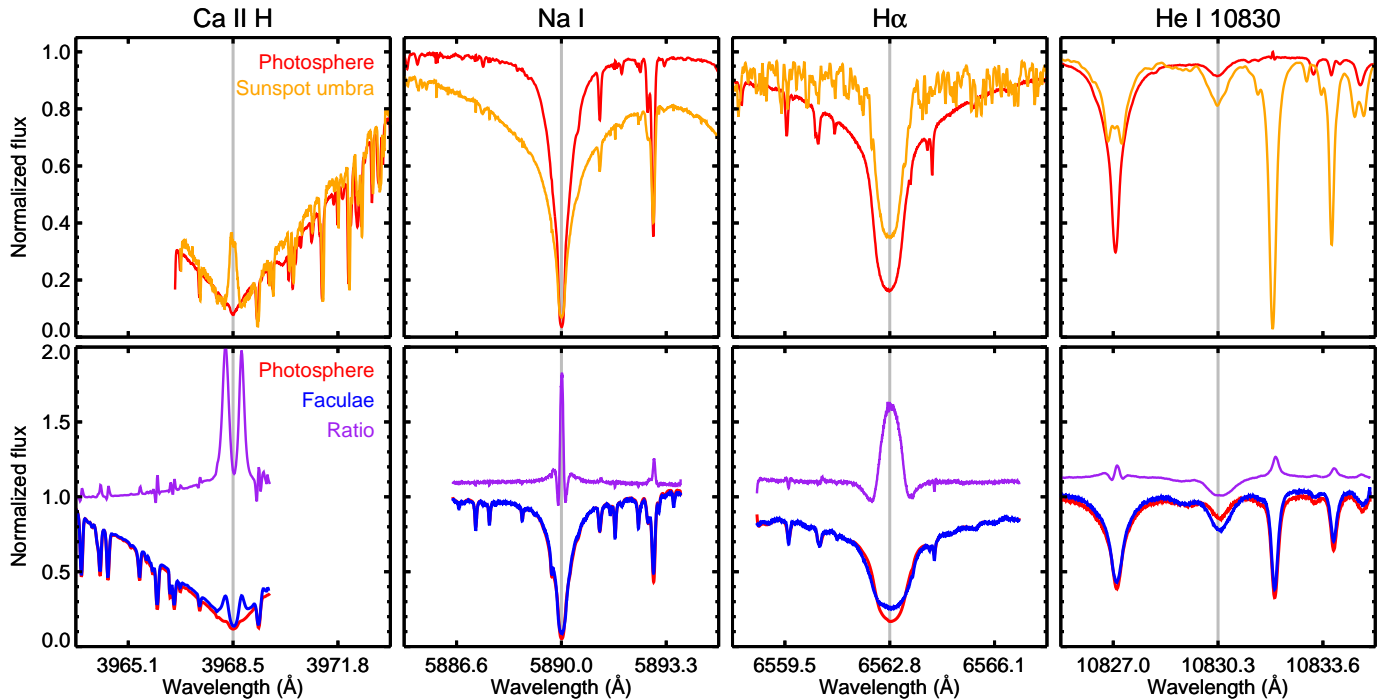
The He I 10830 Å data was acquired in May 2013 with the Tenerife Infrared Polarimeter (TIP-II Collados et al. 2007) attached to the Vacuum Tower Telescope (von der Lühse 1998). The spectrum is an  $10 \times 10$  pixel average taken within an active region, avoiding the sunspot. The Ca II H faculae spectra are extracted from the data presented in Beck & Rezaei (2011, see their Figure 3). Note that we were not able to find suitable Ca II K spectra so Ca II H spectra are used as an approximation. We construct facular spectra by producing a normalized core flux image and then selecting pixels with fluxes  $> 1.5$ . We only use pixels with y-coordinate values  $< 40''$  in order to avoid the solar limb. Spectra from the selected pixels are averaged to produce the facular spectrum in Figure 2. The quiet Sun photosphere spectrum is an average of the pixels with normalized flux values  $0.9 < F_N < 1.1$  in the same region.

Figure 2 shows that faculae-to-photosphere ratios in the line cores, which is represented by  $a_{\text{act}}$  in the simulations, are  $\approx 1.5 - 2.0$  with the largest contrast in Ca II H. The contrast is likely  $\approx 1.5 - 2.0\times$  higher for Ca II K. He I shows the unique behavior among these activity indicators of going further into absorption in facular spectra. Note that the absorption seen in the He I 10830 Å photospheric spectrum is due to the diffuse overlying chromosphere, and is not intrinsic to the photosphere, which could not be completely separated when constructing the line profiles. The enhanced facular absorption is a combination of higher temperatures inducing more collisional excitation and enhanced photoionization by coronal back illumination and subsequent recombination to the lower level of the 10830 Å transition (Andretta & Jones 1997). The enhanced lower level population leads to higher opacity and increased line absorption. We note that for the densest chromospheres in Andretta & Jones (1997) the

<sup>2</sup> <http://diglib.nso.edu/flux>

**Table 1.** Contrast model parameters and explored values

Parameter description	Symbol	Value range
(1)	(2)	(3)
Spot coverage fraction	$f_{sp}$	0.003-0.100
Faculae coverage fraction	$f_{act}$	0.05 - 0.50
Ratio of facular to photosphere core	$a_{act}$	0.5-3.0
FWHM of active region emission/absorption	$\sigma_{act}$	20 km s <sup>-1</sup>
Central latitude of active region distribution	$\theta_{act}$	$\pm 20^\circ - 45^\circ$
Temperature difference between spots and photosphere	$\Delta T_{sp}$	500 - 1500 K
Temperature difference between faculae and photosphere	$\Delta T_{fac}$	50 K
Minimum spot radius	$r_{sp}^{min}$	0.1-0.5 $R_p$
Maximum spot radius	$r_{sp}^{max}$	0.3-1.0 $R_p$
Planet-to-star ratio	$(R_p/R_*)^2$	0.1,0.2



**Figure 2.** Observed solar sunspot (upper row) and faculae (bottom row) spectra. In the upper panel, the spot spectra are normalized to highlight the line core contrast. The faculae-to-photosphere line ratio is shown in purple in the bottom row. The ratio is offset by 0.1 in the Na I, H $\alpha$ , and He I panels. Ratios of  $\approx 1.5 - 2.0$  are seen in Ca II H, Na I, and H $\alpha$ . He I 10830 Å shows absorption relative to the photosphere due to the increased population of He I atoms in the ground state of the 10830 Å transition, the result of the higher temperature in facular regions.

10830 Å transition goes into emission. Energetic solar flares also show He I 10830 Å in emission (Judge et al. 2015; Kuckein et al. 2015). However, the increased absorption in solar facular regions shown here is likely more representative of the average 10830 Å spectrum in the cases discussed in this paper.

Figure 3 shows a transit example using  $(R_p/R_*)^2 = 0.02$  of a narrowband Ca II K solar disk snapshot from the Chromospheric Telescope (ChroTel; Bethge et al.

2011) taken at 13:30:00.00 UT on 2016 July 14. In order to identify spots and active regions in the image, we created a normalized image and assigned points with normalized flux values  $\geq 1.2$  as faculae (bright regions in the image in Figure 3) and  $\leq 0.8$  as spots (darkest regions in Figure 3, e.g., near the active region in the upper-right quadrant). Note that the spot identification also flagged regions that are more likely filaments. These regions contribute negligibly to the total

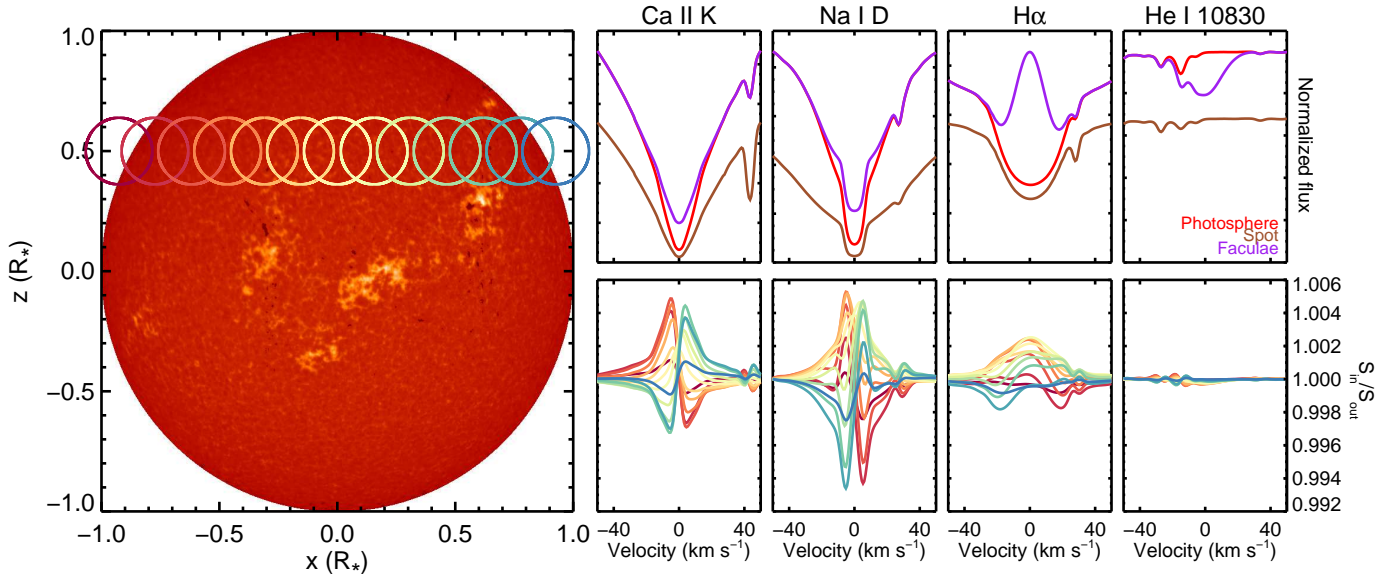


**Figure 3.** Examples of contrast spectra as a function of transit phase for the Sun on 2016 July 14. The solar disk in the left panel is a narrowband Ca II K image rebinned to the spatial resolution ( $0.0025 R_*$ ) used in the simulations. The solar spin axis is in the positive vertical direction. Note that the color scaling is not necessarily representative of the relative brightness of the various features across the disk. The disk shows  $\approx 7\%$  facular coverage and  $\approx 0.2\%$  spot coverage. The colored open circles show the specified planet positions, moving from red to blue as the transit progresses. The upper-right panels show the normalized spectra for the various disk features and spectral lines. The y-axis plot ranges are chosen to highlight the relative core emission strength; the continuum is not necessarily shown. Note that the weak lines blueward of He I 10830 Å are not associated with He I. The bottom-right panels show  $S_T = S_{\text{in}}/S_{\text{out}}$  for the planet positions indicated by the colored circles in the left panel. There is little contribution to  $S_T$  from the active regions; the signal is almost entirely due to CLVs.

flux. This snapshot shows  $\approx 7\%$  facular coverage and  $\approx 0.2\%$  spot coverage, which corresponds to a moderate level of solar activity. We set  $a_{\text{act}} = 1.6$  for Ca II K, H $\alpha$ , and Na I D; for He I 10830 Å  $a_{\text{act}} = -0.2$ . The photospheric and spot spectra are  $T_{\text{eff}} = 5800$  K and  $\Delta T_{\text{sp}} = 500$ , respectively. Note that  $\Delta T_{\text{sp}} = 500$  is more representative of the average brightness temperature of the combined umbral and penumbral regions; the darkest umbral regions in sunspots typically have temperatures  $\approx 1000 - 1500$  K lower than the surrounding photosphere (Sütterlin & Wiehr 1998).

The bottom row of Figure 3 shows the in-transit spectra for the planet positions indicated by the colored circles in the image. For the most part, the only contributions to the contrast spectrum  $S_{\text{in}}/S_{\text{out}}$  are CLVs; the active regions near disk-center do not have much of an effect. The solar example illustrated some important effects. Primarily, stars with a low coverage fraction of active regions will not exhibit a large contrast effect. Also of note is the absence of any contrast signatures at He I 10830 Å;  $a_{\text{act}}$  is smaller in this case compared with the other lines and the contrast spectra are correspondingly weaker. Despite the lack of contrast signatures in the solar case, we explore a wide range of parameters in the following sections in order to understand the possible extent of contrast contamination.

### 3.2. The negligible effect of starspots and filaments

As noted in Cauley et al. (2017a), spots tend to have a small effect on the contrast spectra of the lines explored here. The primary reason for this is the flux-weighted contribution of spots to the integrated spectrum: their cooler temperature produces a smaller fraction of the total flux relative to the same area of photosphere. Note that this is only the case for spot coverage fractions of  $\lesssim 15\%$ . We do not consider larger coverage fractions, such as those explored in Rackham et al. (2018), since there is no evidence of such large spot areas in main sequence G and K stars.

Figure 4 shows an example for stellar surfaces with a spot coverage fraction of 10%. The red lines show the  $(R_p/R_*)^2 = 0.01$  case and the blue lines show the 0.02 case. The absorption is measured across a 2 Å band, centered on the rest wavelength of the line, of the mean  $S_{\text{in}}/S_{\text{out}}$  spectrum across the stellar disk. Note that the absorption is in *parts per million*. Figure 4 demonstrates how small the contrast effect is from spots for atomic lines, independent of  $\Delta T_{\text{sp}}$ . While it is possible that transits of spot groups may produce larger signals for a small portion of the transit, consistent in-transit absorption signatures are unlikely to be due to star spots. Furthermore, the strength of atomic absorption typically detectable in high-resolution transmission spectra is  $\approx 0.1\%$ , about 10 – 1000 $\times$  the strength of the

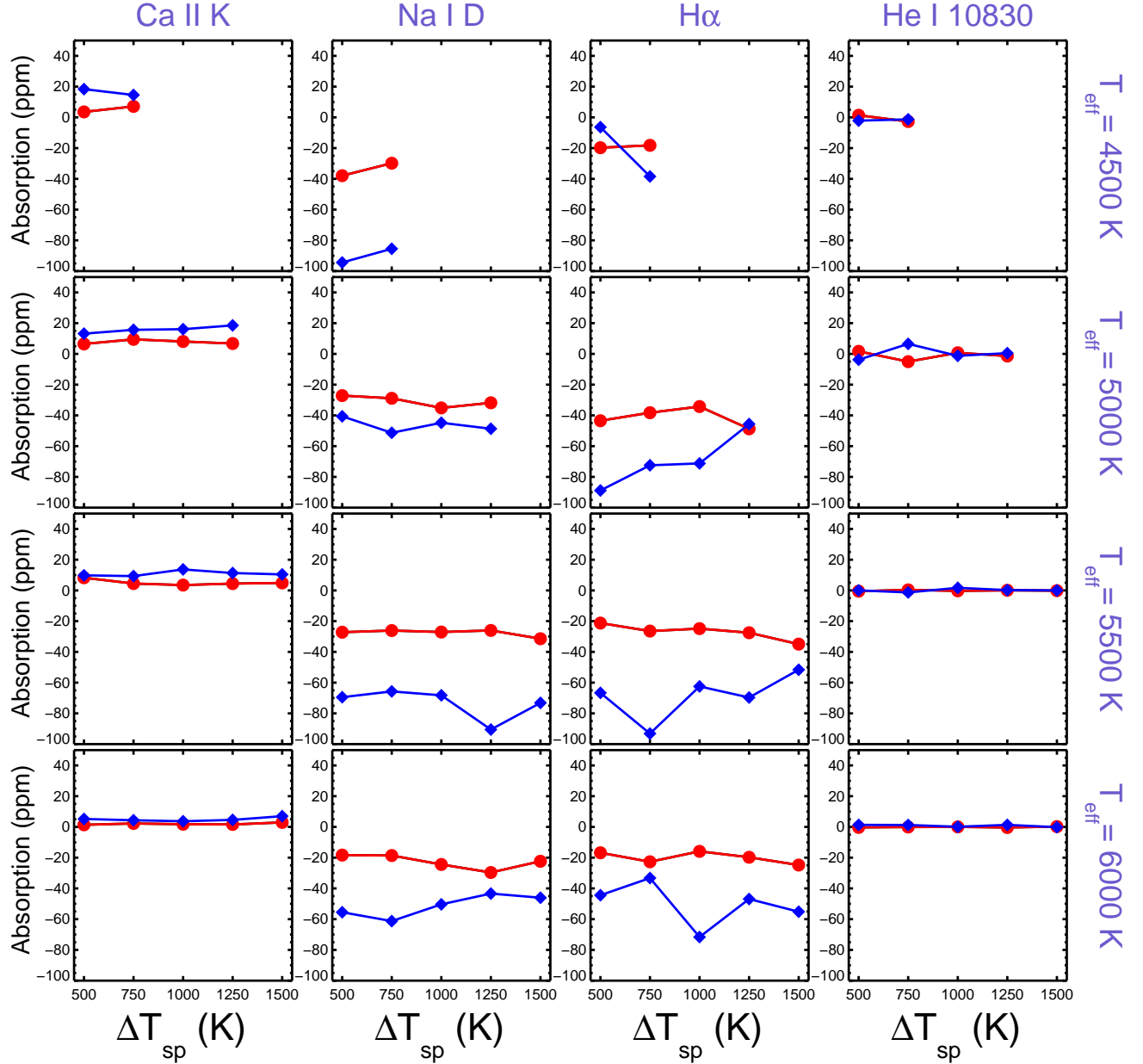


**Figure 4.** Mean in-transit absorption signatures for stellar surfaces with  $f_{\text{sp}} = 10\%$  as a function of  $\Delta T_{\text{sp}}$  (see Section 2 for details on the choice of  $\Delta T_{\text{sp}}$ ). Columns are individual lines and rows show the same  $T_{\text{eff}}$ . The red lines are for  $(R_p/R_*)^2 = 0.01$  and the blue lines represent  $(R_p/R_*)^2 = 0.02$ . The absorption in the line is measured in parts per million (ppm) and all cases are shown with the same absorption range of  $-100$  to  $50$  ppm for comparison. None of the cases shown exhibit any contrast effect above  $\approx 0.01\%$ , even for this extreme example of a  $10\%$  coverage fraction.

contamination found here for the pure spot case. Thus it not currently feasible to disentangle such small effects from the measurements. The active region scenarios explored in the rest of the paper all include a  $0.3\%$  spot coverage fraction for completeness.

Filaments are embedded in the chromosphere and corona and are made of cool material when compared to their surroundings (Martin 1998). Magnetic field lines

support them against gravity. They appear in absorption against the solar disk but are seen as bright prominences when observed above the limb. We explored the magnitude of the contrast effect due to filaments in Cauley et al. (2017a) and found them to be unimportant compared to faculae and spots. Thus we ignore them here and refer the reader to our previous work for more details.

### 3.3. Uniform distribution of active regions

One broad category of active region coverage is a uniform distribution across the stellar disk. Figure 5 shows a  $(R_p/R_*)^2 = 0.02$  transit example for  $f_{\text{act}} = 0.4$ , the active region coverage fraction, and  $a_{\text{act}} = 3.0$  ( $-0.4$  for He I 10830 Å), the flux relative to that in the line core of the photospheric spectrum. Note that the He I 10830 Å contrast spectra show *emission*, the opposite of the other lines. We do not show the emission and absorption components of the lines for spot spectra (see Figure 2 for the solar case); only the scaled model spectrum of the appropriate spot  $T_{\text{eff}}$  is given for clarity.

Figure 6 and Figure 7 show absorption maps for the  $(R_p/R_*)^2 = 0.01$  and  $(R_p/R_*)^2 = 0.02$  cases, respectively. The color bars show the absorption, in percent, measured for the mean  $S_{\text{in}}/S_{\text{out}}$  spectrum sampled across the transit. The strength of the contrast absorption roughly increases as  $a_{\text{act}}$  and  $f_{\text{act}}$  increase, i.e., from the lower-left to the upper-right of each map. This can be seen most clearly for the cases of Na I D with  $T_{\text{eff}} = 4500$  K and H $\alpha$  with  $T_{\text{eff}} = 5500$  K. However, absorption from the contrast effect is  $\lesssim 0.005\%$  for all lines and the difference between even the largest and smallest values is  $\approx 0.005\%$ . The weak absorption in the uniform case is dominated by noise, with small variations in the location of active regions producing random changes in the measured absorption. This suggests that a consistent in-transit absorption signal measured for a transiting exoplanet is unlikely to be caused by a uniform active region distribution.

### 3.4. Active latitudes

In Cauley et al. (2017a) we showed that the only scenario capable of producing the observed in-transit H $\alpha$  transmission spectrum for HD 189733 b was the transit of a very active latitude. To produce a consistent in-transit absorption signature, the planet must continuously transit active regions with similar activity levels, i.e., chromospheric emission or absorption. Here we extend the active latitude analysis to all of the lines and a broader range of active region parameters.

Figure 8 shows an example of an active latitude transit for a transit chord centered on the active latitude. This is critical: the average contrast spectrum depends strongly on whether or not the planet transits within  $\approx \pm 5^\circ$  of the active latitude center. Off-latitude transits are explored in Section 3.5. It is clear from Figure 8 that the contrast spectra are much stronger than in the uniform distribution case (see Figure 6 and Figure 7).

One noteworthy feature in Figure 8 is the behavior of He I 10830 Å: because this line is in absorption in most normal stellar chromospheres, transits of active regions seen at 10830 Å will show *emission* instead of absorption. This suggests that any He I 10830 Å atmospheric absorption signatures will tend to be masked by the contrast effect, not enhanced. This is encouraging for He I 10830 Å transmission spectra since detections will likely

be lower limits and can confidently be attributed to the planet’s atmosphere and not to stellar active regions.

Figure 9 and Figure 10 show the absorption maps for active latitude transits. The absorption increases approximately linearly with  $a_{\text{act}}$  and  $f_{\text{act}}$ . There is little variation with  $T_{\text{eff}}$ , suggesting that the contrast effect is not strongly affected by the underlying photospheric spectrum but rather the strength and distribution of active regions. The strongest absorption signatures are seen in the  $(R_p/R_*)^2 = 0.02$  case for H $\alpha$  and Na I D, which are  $\approx 0.35\%$  and  $\approx 0.18\%$ , respectively. Comparisons of the contrast simulation absorption to observed values will be discussed in Section 4.

We note that the absorption in the  $(R_p/R_*)^2 = 0.01$  case is not necessarily 50% of that in the  $(R_p/R_*)^2 = 0.02$  case. Figure 11 shows the absorption ratio for the  $(R_p/R_*)^2 = 0.01$  and  $0.02$  simulations in the case of  $a_{\text{act}} = 3.0$  and  $f_{\text{act}} = 0.4$ . The ratio is not exactly 0.5 and tends to increase with  $T_{\text{eff}}$ . Although we have not been able to isolate the cause of this trend, it is likely due to differences in limb darkening curves as a function of  $T_{\text{eff}}$ .

### 3.5. Transiting away from active latitudes

We showed in Section 3.4 that transits of active latitudes can produce significant contrast signatures in certain cases. However, those cases were for active regions distributed normally around the planet’s transit latitude. This increases the likelihood that the planet covers active regions and produces a contrast signal. Here we explore how the contrast effect changes as the active region latitude moves away from the planet’s transit latitude.

Figure 12 shows an example of an off-latitude transit and Figure 13 shows the contrast absorption as a function of active region latitude with a planet transit latitude of  $30^\circ$  ( $b = 0.5$ ) and  $(R_p/R_*)^2 = 0.02$ . For this example we fix the active region coverage fraction and facular core ratio to  $f_{\text{fac}} = 0.35$  and  $a_{\text{act}} = 3.0$ , respectively. For He I 10830 Å we use  $a_{\text{act}} = -0.4$ . These values were chosen because they produce strong contrast spectra in the active latitude transit case.

For each spectral line the contrast absorption decreases sharply as the active region latitude moves away from the planet’s transit latitude. This suggests that in order to produce significant contrast signals active latitudes need to be centered within  $\leq 5^\circ$  from the planet’s transit latitude. The need for the planet to transit very close to the active latitude argues against consistent in-transit absorption signatures being produced by the contrast effect. For this to be the case, the active latitude must cover almost the entire circumference of the star at the planet’s transit latitude. Furthermore, the active belt cannot migrate away from the transit chord, which is unlikely if the star experiences activity cycles comparable to the Sun. The simulations presented here

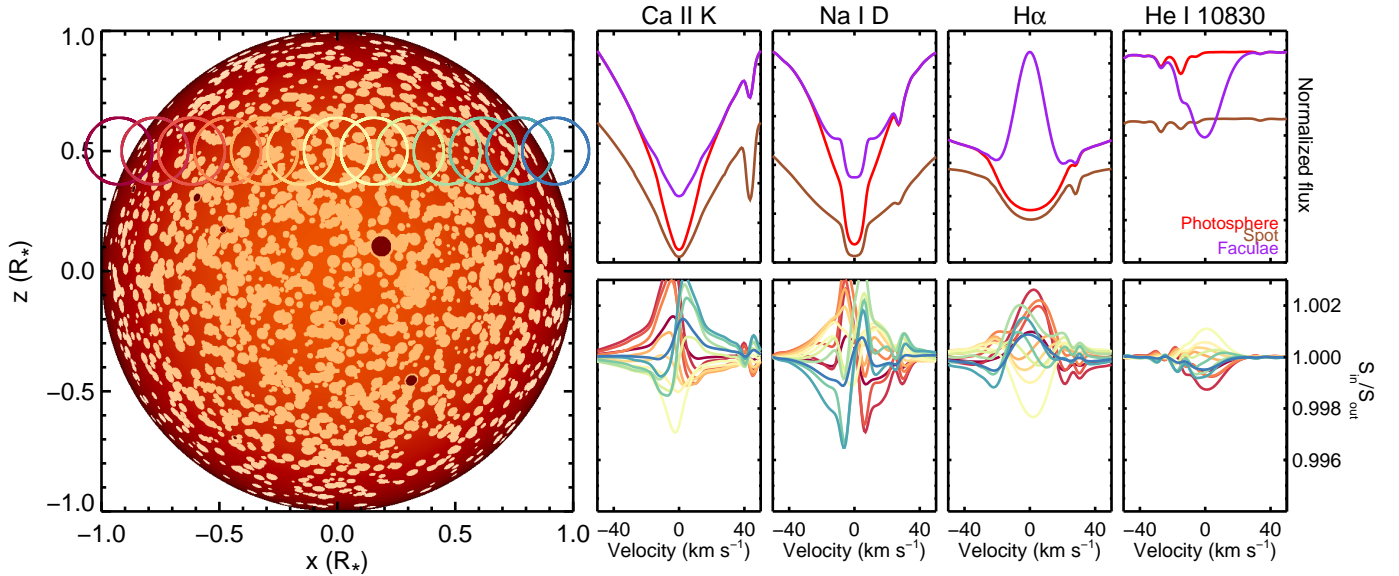


**Figure 5.** Same format as [Figure 3](#) except for a simulated uniform distribution of active regions. Note that colors do not accurately represent the relative brightness of surface features and are used for illustrative purposes. The example shows the case of  $f_{\text{act}} = 0.4$ ,  $a_{\text{act}} = 3.0$  ( $-0.4$  for He I 10830 Å),  $(R_p/R_*)^2 = 0.02$ , and  $T_{\text{eff}} = 5500$  K. The left panel shows the stellar disk configuration, with light regions representing active regions, darker regions representing spots, and the open colored circles showing the planet positions at which contrast spectra are calculated. The upper-right panels show the normalized photospheric, spot, and faculae spectra for each line. The bottom-right panels show the contrast spectra  $S_{\text{in}}/S_{\text{out}}$  as a function of transit phase, where the colors map to those in the stellar disk image. The strongest effect can be seen mid-transit where the contrast spectra can reach depths of  $\approx 0.5\%$  and absorption values of  $\approx 0.02\%$ .

thus confirm the result in [Cauley et al. \(2017a\)](#) for the in-transit H $\alpha$  signal observed for HD 189733 b.

#### 4. DISCUSSION

Our simulations show that the contrast effect for chromospheric lines in the optical can be non-negligible for certain active region configurations and intrinsic emission strengths. Randomly distributed active regions, however, even in cases of coverage fractions of  $\approx 50\%$ , cannot produce strong contrast spectra. Active latitudes centered  $\leq 5^\circ$  from the planet’s transit latitude are necessary to create contrast absorption lines with central depths of  $\approx 1\%$ .

How do the strongest contrast scenarios compare with observations? [Table 2](#) lists the current published absorption detections for Na I D and H $\alpha$ . We do not include comparisons for Ca II K and since there are no reported detections for Ca II K in the literature that can be attributed to atmospheric absorption<sup>3</sup>. Furthermore, the absorption cores of these lines are most strongly affected by NLTE effects, which we do not account for. The only He I 10830 Å detection ([Spake et al. 2018](#)) is given its own discussion below. The bottom of the table lists the Na I 5890 Å and H $\alpha$  values obtained for the case of

$(R_p/R_*)^2 = 0.02$  and  $T_{\text{eff}} = 5500$  K and  $a_{\text{act}} = 3.0$ . The value of  $f_{\text{act}}$  is given in brackets.

Even the extreme case of  $f_{\text{act}} = 0.5$  for uniformly distributed active regions cannot account for 10% of the absorption in any of the published values. Similarly, off-latitude transits can only produce up to  $\approx 50\%$  of the observed values. Contrast absorption for active latitude transits, however, approaches the published values for both Na I D and H $\alpha$ . Absorption as strong as  $\approx 1\%$ , such as that detected in Na I D for WASP-49 b ([Wytenbach et al. 2017](#)) and WASP-69 b ([Casasayas-Barris et al. 2017](#)) is still well above the maximum values found in our simulations.

While our simulations show that it may be possible to produce contrast signatures similar to what is observed in HD 189733 b, as suggested by [Barnes et al. \(2016\)](#), we argue that this is unlikely. As we have seen, in order to produce the strongest contrast signatures the planet must be transiting very close to the central latitude of an active band on the stellar surface. In addition, the strength of the intrinsic emission in the active regions must be  $\approx 2\times$  that seen in solar active regions. Finally, this same scenario must persist across many epochs in order to consistently produce in-transit absorption, such as is repeatedly observed for HD 189733 b in both H $\alpha$  and Na I D ([Redfield et al. 2008](#); [Jensen et al. 2011](#); [Wytenbach et al. 2015](#); [Khalafinejad et al. 2017](#); [Cauley et al. 2017a](#)). The specificity of the necessary active re-

<sup>3</sup> See [Cauley et al. \(2017a\)](#) for possible in-transit Ca II H and K absorption signatures

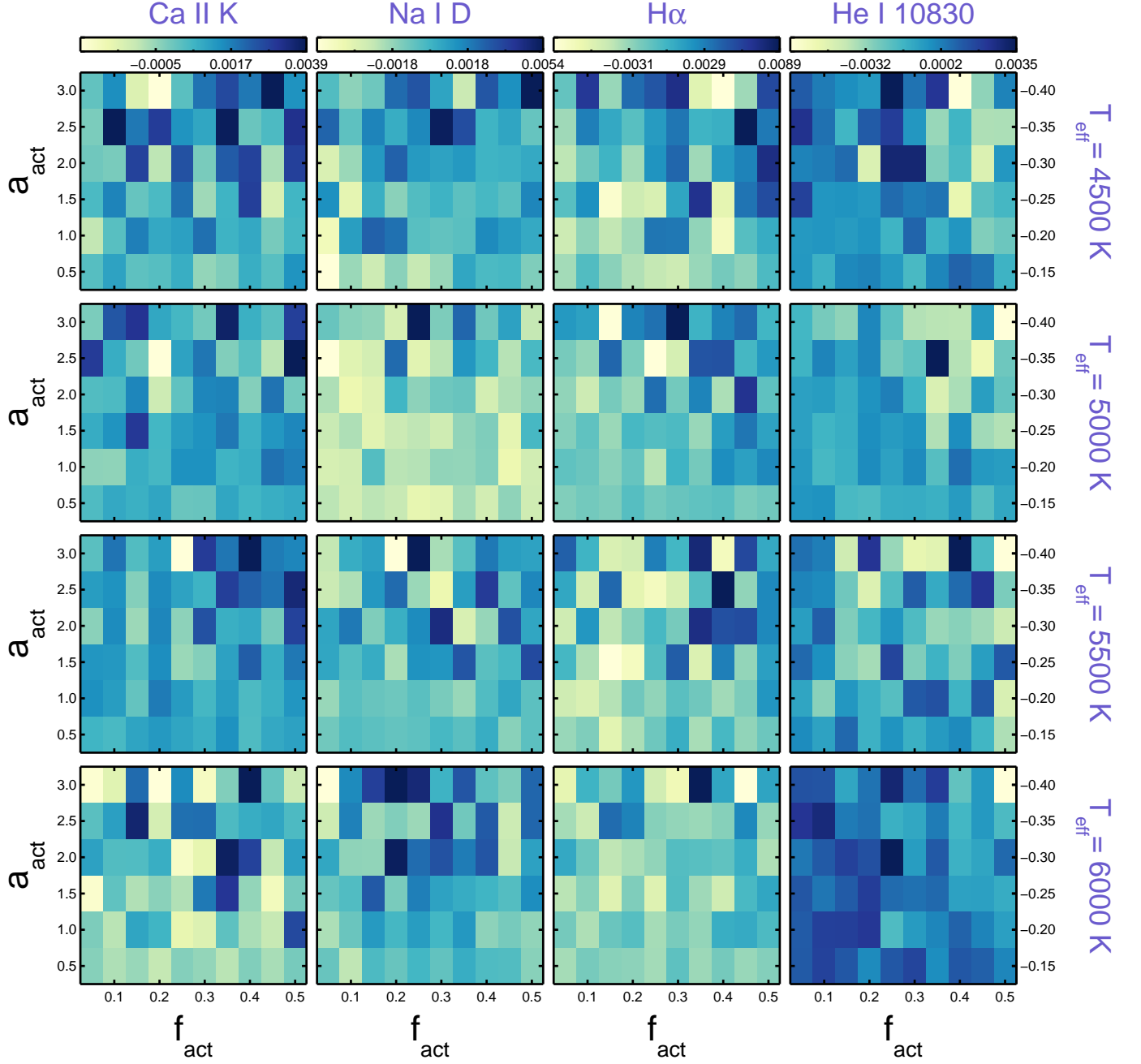


**Figure 6.** Mean in-transit absorption for transits of a stellar disk with a uniform distribution of active regions for the case of  $(R_p/R_*)^2 = 0.01$ . Columns are individual lines and rows are  $T_{\text{eff}}$ . The x-axis  $f_{\text{act}}$  is the active region coverage fraction of the stellar disk and the y-axis  $a_{\text{act}}$  is the strength of the active region emission. Note that the He I 10830 Å vertical scale is different from the other lines. The values indicated by the color bars are in percent absorption (integrated over  $\lambda_0 \pm 1 \text{ \AA}$ ). All panels are on the same absolute color scale. The effects are almost entirely negligible for most lines, suggesting that even large active region coverage fractions cannot produce strong contrast signals if they are uniformly distributed.

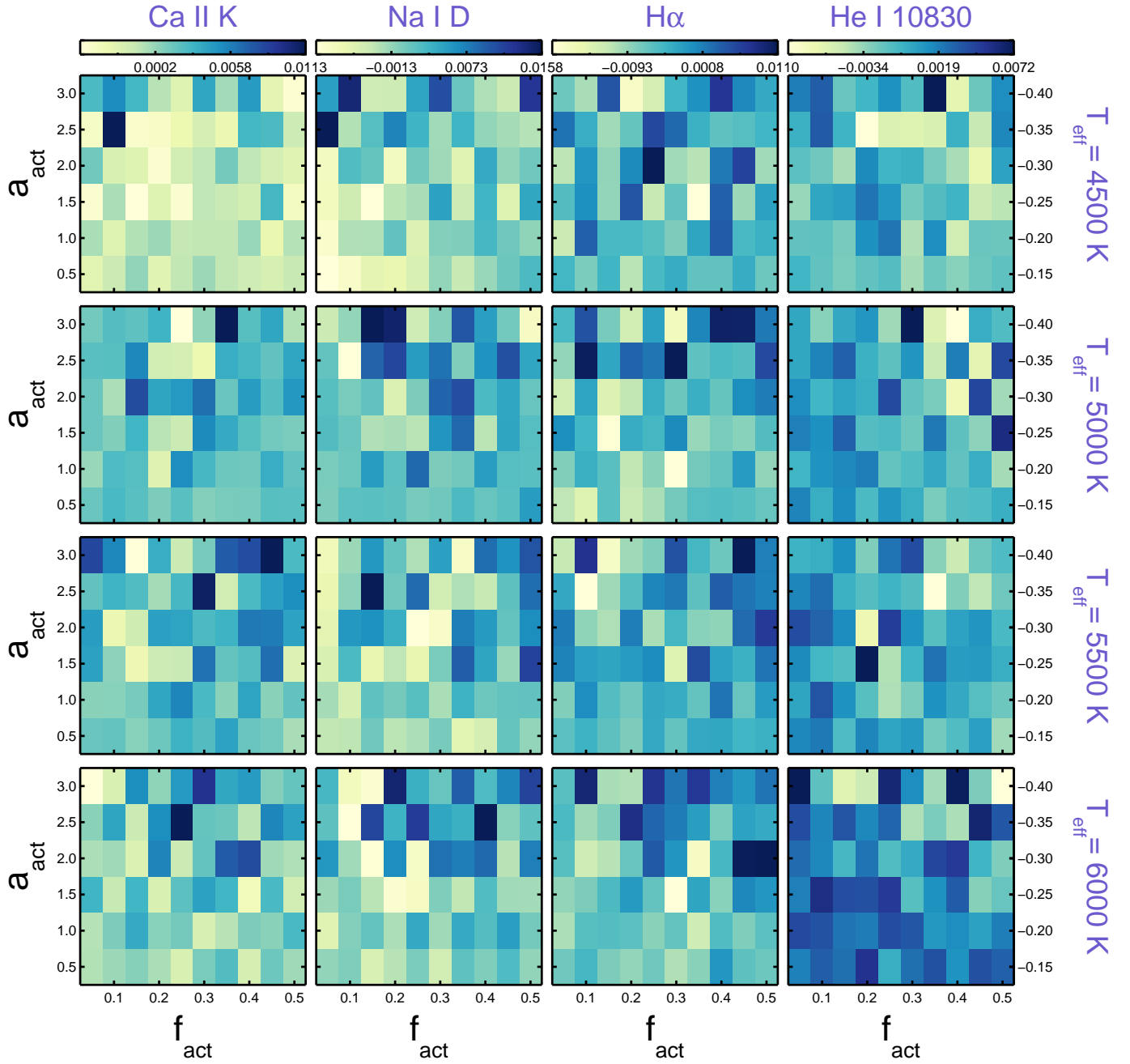


**Figure 7.** Same as Figure 6 but for a uniform distribution of active regions for the case of  $(R_p/R_*)^2 = 0.02$ . Similar to the  $(R_p/R_*)^2 = 0.01$  case, the effects are small, never reaching values greater than  $\approx 0.006\%$ .

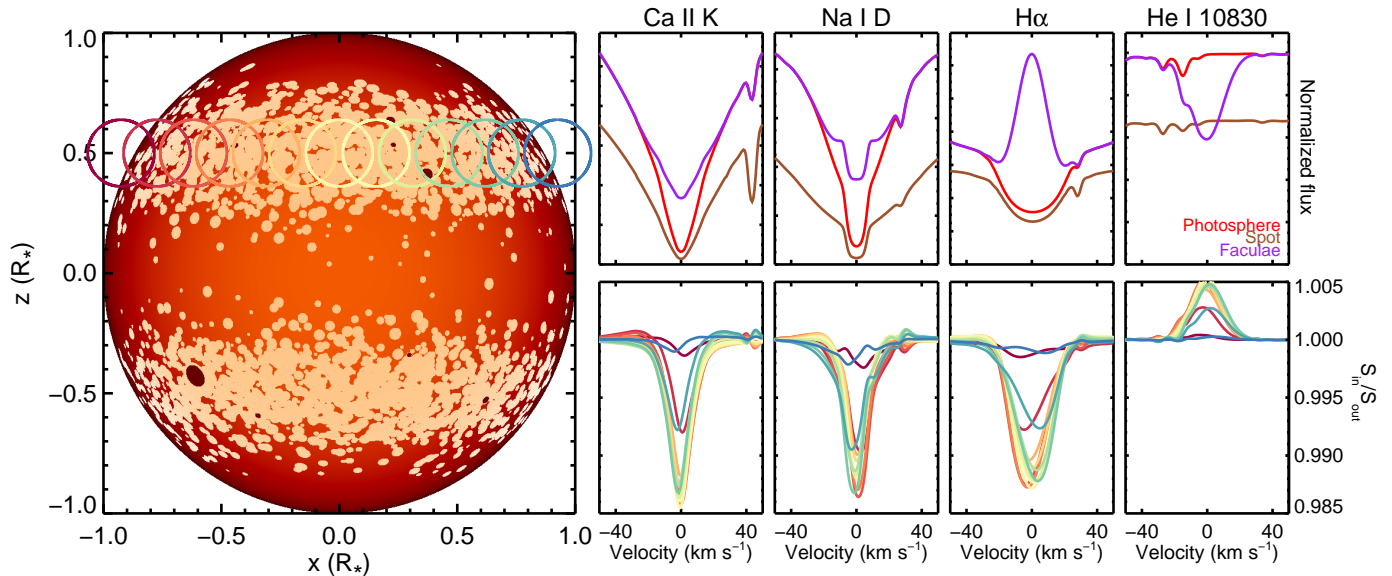


**Figure 8.** Examples of contrast spectra as a function of transit phase for an active latitude case. The parameters used and the format is the same as Figure 5 except the active regions are distributed normally around the planet’s transit latitude. The contrast effect is much stronger due to the constant occultation of faculae by the planet.

gion parameters argues against the contrast effect as the mechanism responsible for the transmission absorption measured for planets transiting active stars. Nonetheless, a small fraction of the measured absorption is likely due to the transiting of stellar active regions. This should be taken into consideration when considering discussions of  $H\alpha$  transmission spectra.

The usefulness of He I 10830 Å as a diagnostic of exoplanetary exospheres was recently reignited by Oklopčič & Hirata (2018) (see also Seager & Sasselov 2000; Turner et al. 2016). Soon after, the first detection of He I 10830 Å in an exoplanet atmosphere was reported by Spake et al. (2018) for WASP-107 b. Our simulations suggest that He I 10830 Å transmission absorption can be contaminated at the 0.1% level for transits of active latitudes. However, any exosphere absorption should be *decreased* by the planet’s transit of active regions since He I 10830 Å is mostly in absorption in G and K star active regions. The only exception to this would be for very dense chromospheres which show He I 10830 Å in emission, an unlikely scenario even for main-sequence M-dwarfs (Andretta & Jones 1997).

The relative absorption signature measured by Spake et al. (2018) is 0.049% integrated over 98 Å. A similar integration bin for our simulated He I 10830 Å contrast spectra, in the case of an active latitude transit for  $f_{\text{act}} = 0.40$ ,  $a_{\text{act}} = -0.40$ ,  $T_{\text{eff}} = 4500$  K, and  $(R_p/R_*)^2 = 0.02$ , gives an emission contribution to the contrast spectrum of  $\approx -0.004\%$ . This is  $\approx 10\times$  lower than the magnitude of the WASP-107 b measurement and is in emission instead of absorption. Thus the signal from Spake et al. (2018) may be diluted at the  $\approx 10\%$  level but, as Spake et al. (2018) also discuss, cannot be

the cause of transiting a quiet photospheric chord. Due to the small contrast effect in the line, He I 10830 Å should be considered favorable compared with  $H\alpha$  or Na I D as a transmission spectroscopy tool for probing extended exoplanet atmospheres.

$H\alpha$  remains an under-utilized tool for probing the thermospheres of hot planets. The presence of  $n = 2$  hydrogen in hot planet atmospheres is well-established theoretically (Christie et al. 2013; Huang et al. 2017). Due to its ease of access with echelle spectrographs, the somewhat higher signal-to-noise in the line core compared with Na I D, and the fact that it is relatively free of telluric contamination, combined with our findings that even active stars most likely cannot produce strong contrast spectra,  $H\alpha$  should be considered in future transmission spectroscopy studies of hot planets. This is especially the case for extremely hot planets such as KELT-9 b (Gaudi et al. 2017) and KELT-20 b (Lund et al. 2017) where the temperature is high enough for collisional excitation of hydrogen to become important (Huang et al. 2017).

## 5. CONCLUSION

We have explored how stellar activity in the form of spots and bright facular or plage regions can contribute to the high-resolution optical transmission spectra in chromospherically active lines for giant planets. Overall, the emission from stellar active regions in the simulated lines has a weak effect on the transmission spectrum and varies little with  $T_{\text{eff}}$ . Only specific geometries, where the active region distribution is within  $\approx 5^\circ$  of the planet’s transit chord, combined with coverage fractions  $\gtrsim 20\%$  and active region emission strengths  $2 - 3\times$  the photospheric line strength can produce signatures sim-

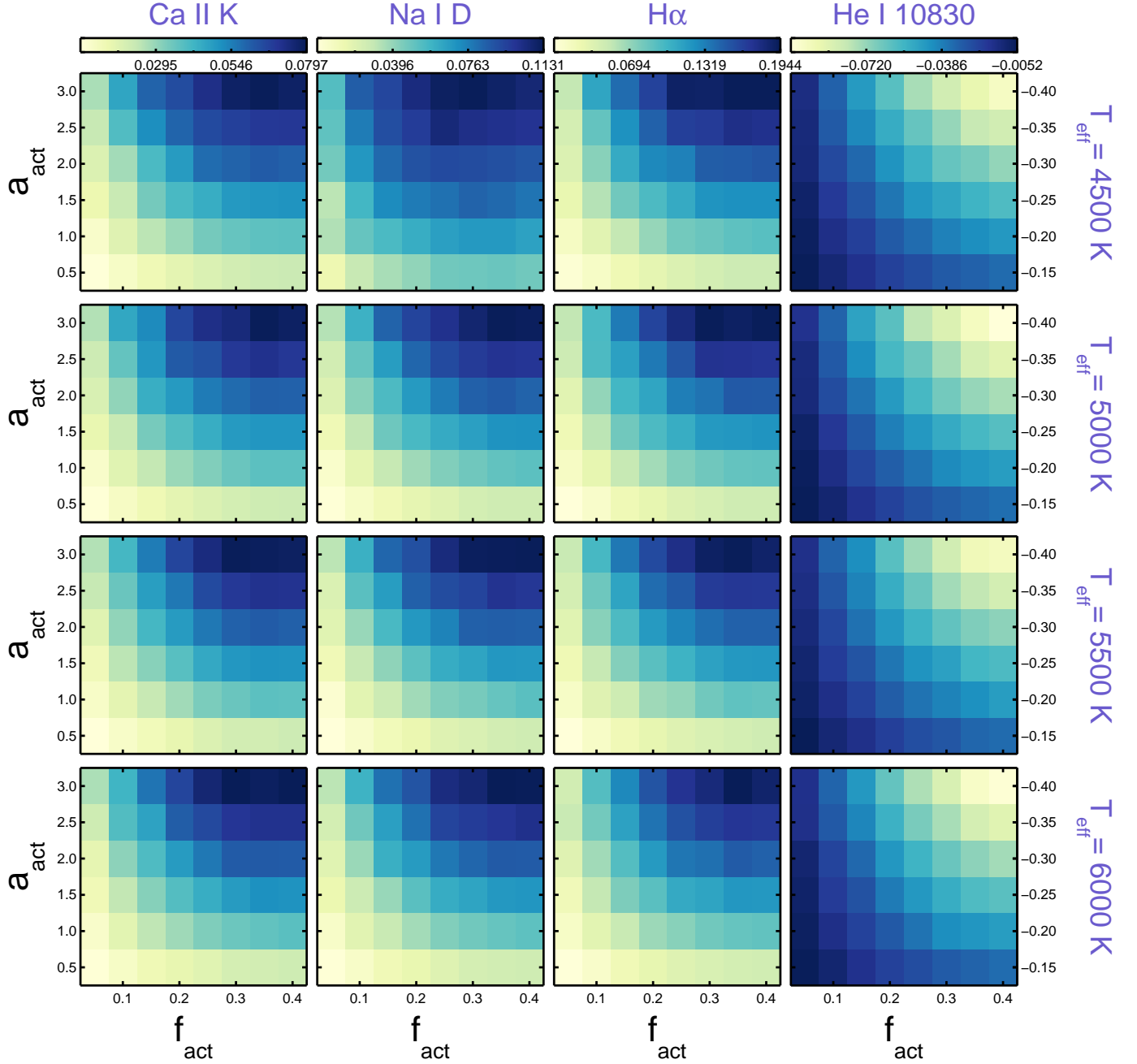


**Figure 9.** Example of absorption maps for active latitude transits for the case of  $(R_p/R_*)^2 = 0.01$ . All formatting is the same as Figure 6. The effects are much larger than the uniform cases (Figure 6 and Figure 7), although still small for most lines. The contamination values for Na I D approach 0.1%, a non-negligible fraction of the measured absorption in some exoplanet atmospheres.

ilar to those observed for certain hot planet systems. In particular, observed  $H\alpha$  and Na I D absorption can most likely be attributed to the planet’s atmosphere in the case of HD 189733 b, although some of the signal probably originates in stellar active regions, especially in the case of  $H\alpha$ .

He I 10830 Å is a promising exosphere diagnostic (Spake et al. 2018) and we find that atmospheric ab-

sorption should be depressed relative to the true values due to He I 10830 Å being in absorption in stellar chromospheres. However, the effect is on the order of  $\approx 0.1\%$  even for active region coverage fractions of  $\approx 0.4$ , suggesting that stellar activity should be unimportant for exoplanets with moderate predicted He I 10830 Å absorption (e.g., GJ 436 b and HD 209458 b; Oklopčić & Hirata 2018). This strengthens the case for the utility

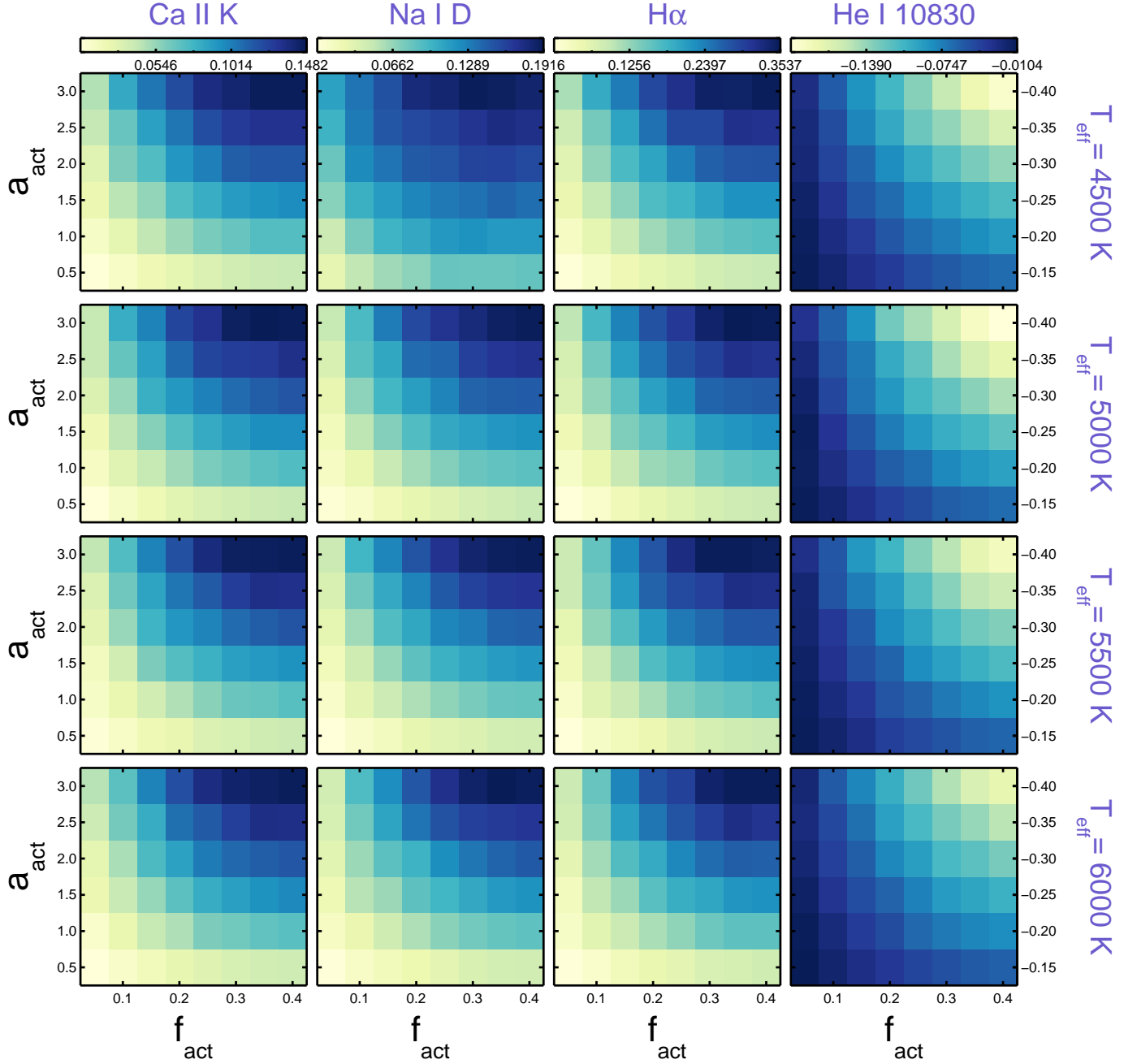


**Figure 10.** Example of absorption maps for active latitude transits for the case of  $(R_p/R_*)^2 = 0.02$ . All formatting is the same as Figure 6. The magnitude of the contrast contamination is  $\approx 2\times$  the amount seen in the  $(R_p/R_*)^2 = 0.01$  case and approaches observed values for the most extreme cases (upper-right corners of each map; see Table 2 for observed values of H $\alpha$  and Na I D).

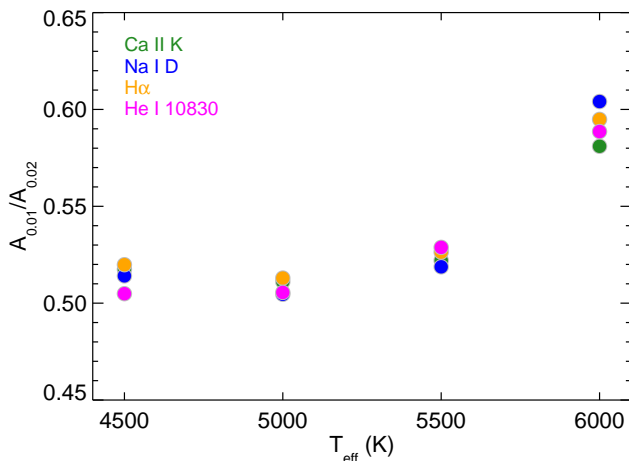
of the 10830 Å line as a diagnostic of exoplanet atmospheres.

The era of extremely large telescopes (ELTs) will enable high-resolution transmission spectra of super-Earths and small rocky planets. The effects of planets transiting active regions scales with the value of  $(R_p/R_*)^2$ , suggesting that the relative magnitude of the contrast effect should be similar for super-Earths and

rocky planets. However, transmission spectrum light curves will likely exhibit higher levels of temporal variability since the relative size of the planet to spots and active regions decreases, increasing the frequency with which the planet transits individual active regions. Simulations of the contrast effect for super-Earths and rocky planets should be pursued.

**Table 2.** Observed atomic transmission spectra absorption

Reference	Object	$R$ ( $\lambda/\Delta\lambda$ )	Integration bin ( $\text{\AA}$ )	Na I D $\text{\AA}$ (%)	H $\alpha$ (%)
(1)	(2)	(3)	(4)	(5)	(6)
Charbonneau et al. (2002)	HD 209458 b	5540	1.2	0.023	...
Snellen et al. (2008)	HD 209458 b	45,000	1.5	0.07	...
Redfield et al. (2008)	HD 189733 b	60,000	12.0	0.067	...
Jensen et al. (2011)	HD 189733 b	60,000	12.0	0.053	...
Jensen et al. (2012)	HD 189733 b	60,000	6.0	...	0.302
Cauley et al. (2015)	HD 189733 b	68,000	2.0	...	0.293
Wytttenbach et al. (2015)	HD 189733 b	115,000	1.5	0.141	...
Cauley et al. (2016)	HD 189733 b	68,000	2.0	0.082	0.685
Khalafinejad et al. (2017)	HD 189733 b	60,000	1.5	0.340	...
Wytttenbach et al. (2017)	WASP-49 b	115,000	0.4	1.440	...
Chen et al. (2017)	WASP-52 b	1100	16.0	0.378	...
Casasayas-Barris et al. (2017)	WASP-69 b	115,000	1.5	5.8	...
Casasayas-Barris et al. (2018)	KELT-20 b	115,000	0.75	0.178	0.594
Uniform [ $f_{\text{act}} = 0.50$ ]	$(R_p/R_*)^2 = 0.02$	70,000	2.0	-0.003	< 0.001
Active latitude [ $f_{\text{act}} = 0.40$ ]	$(R_p/R_*)^2 = 0.02$	70,000	2.0	0.183	0.325
Off-latitude [ $f_{\text{act}} = 0.35$ ]	$(R_p/R_*)^2 = 0.02$	70,000	2.0	0.059	0.111

**Figure 11.** Absorption ratio between  $(R_p/R_*)^2 = 0.01$  and  $0.02$  for the active latitude case of  $a_{\text{act}} = 3.0$  and  $f_{\text{act}} = 0.4$ . The ratio is not exactly 0.5 and tends to increase with increasing  $T_{\text{eff}}$ .

While we have attempted to explore a broad parameter space for giant planet transits of active stellar surfaces, we caution against specific comparisons of exoplanet systems with absorption values derived here. More precise knowledge of the active region distributions and emission strength for exoplanet host stars is needed to reach firmer conclusions about the absolute contribution of active regions to exoplanet transmission spectra. Magnetic mapping and modeling of faculae and

spot contributions to the spectra and brightness variations of planet hosting stars will be useful in this respect (e.g., Dumusque et al. 2014; Herrero et al. 2016; Fares et al. 2017). Non-LTE effects should also be included in order to produce more precise estimates of the contrast effect in specific spectral lines.

**Acknowledgments:** We thank the anonymous referee for their comments and suggestions, which helped improve the manuscript. This work is supported by NASA Origins of the Solar System grant No. NNX13AH79G (PI: E.L.S.). A portion of this work is also supported by the National Science Foundation through Astronomy and Astrophysics Research Grant AST-1313268 (PI: S.R.). CD, CK, and MV were supported by grant DE 787/5-1 of the Deutsche Forschungsgemeinschaft (DFG). This work has made use of NASA’s Astrophysics Data System. Vacuum Tower Telescope in Tenerife and ChroTel are operated by the Kiepenheuer-Institute for Solar Physics, Freiburg, Germany, at the Spanish Observatorio del Teide, of the Instituto de Astrofísica de Canarias. The ChroTel filtergraph has been developed by the Kiepenheuer-Institute in co-operation with the High Altitude Observatory in Boulder, CO, USA.

*Software:* SPECTRUM, Gray & Corbally (1994), <http://www.appstate.edu/grayro/spectrum/spectrum.html>

## REFERENCES

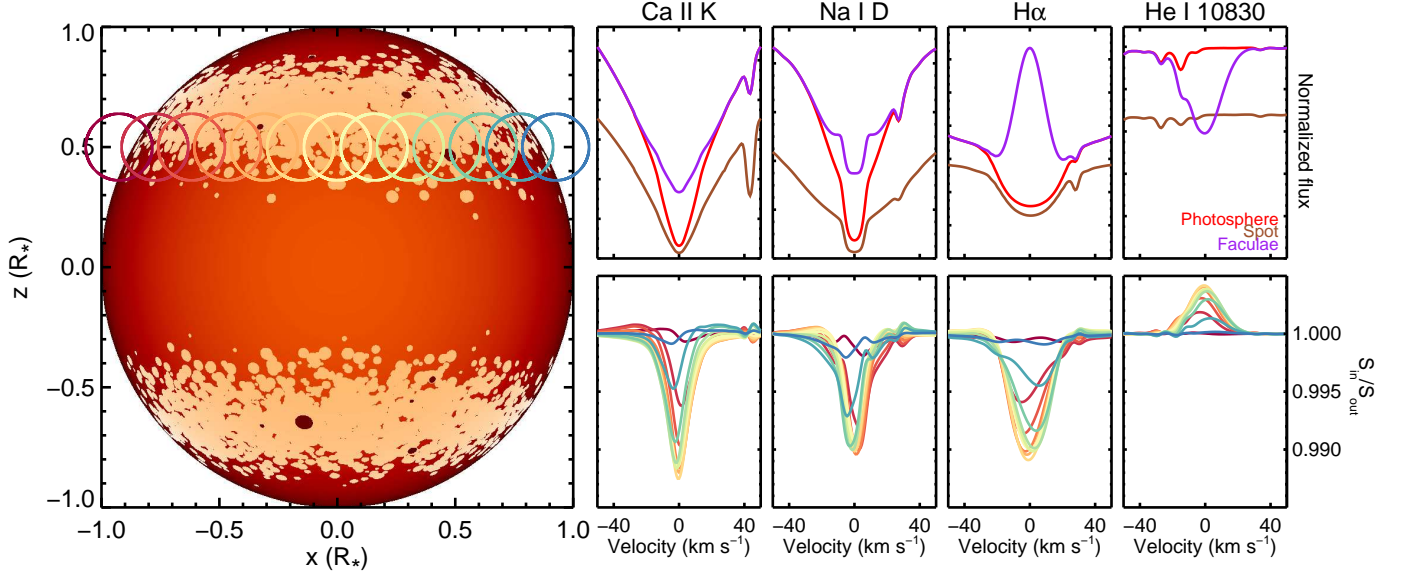


**Figure 12.** Examples of contrast spectra as a function of transit phase for a transit  $\approx 10^\circ$  off the center of an active latitude. The parameters used and the format is the same as Figure 5. The active latitudes are at  $\pm 40^\circ$ . The contrast effect is weaker compared with the active latitude case in Figure 10 since the planet transits portions of the disk with a lower density of active regions.

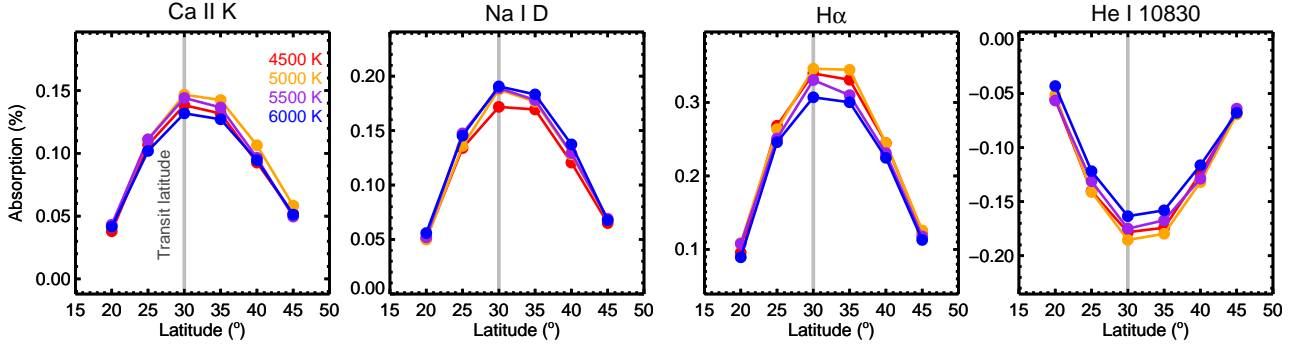


**Figure 13.** Contrast absorption as a function of central latitude for active latitudes. Colors represent  $T_{\text{eff}}$  and the planet's transit latitude is shown with the vertical gray line. Note that more negative numbers imply a stronger effect for He I 10830 Å. The contrast absorption decreases sharply when the active latitudes are centered away from the planet's transit latitude.

Andretta, V., Giampapa, M. S., Covino, E., Reiners, A., & Beek, B. 2017, *ApJ*, 839, 97

Barnes, J. R., Haswell, C. A., Staab, D., & Anglada-Escudé, G. 2016, *MNRAS*, 462, 1012

Beck, C. A. R., & Rezaei, R. 2011, *A&A*, 531, A173

Beek, B., Schüssler, M., Cameron, R. H., & Reiners, A. 2015, *A&A*, 581, A43

Berdugina, S. V. 2005, *Liv. Rev. Sol. Phys.*, 2, 8

Berger, T. E., Rouppe van der Voort, L., & L'ofdahl, M. 2007, *ApJ*, 661, 1272

Berta, Z. K., Charbonneau, D., Bean, J., et al. 2011, *ApJ*, 736, 12

Bethge, C., Peter, H., Kentischer, T. J., et al. 2011, *A&A*, 534, 105

Bourrier, V., Lecavelier des Etangs, A., & Vidal-Madjar, A. 2015, *A&A*, 573, A11

Brogi, M., de Kok, R. J., Albrecht, S., et al. 2016, *ApJ*, 817, 106

Casasayas-Barris, N., Palle, E., Nowak, G., et al. 2017, *A&A*, 608, 135

Casasayas-Barris, N., Palle, E., Yan, F., Chen, G., et al. 2018, accepted to *A&A*

Cauley, P. W., Redfield, S., Jensen, A. G., et al. 2015, *ApJ*, 810, 13

- Cauley, P. W., Redfield, S., Jensen, A. G., & Barman, T. 2016, *AJ*, 152, 20
- Cauley, P. W., Redfield, S., & Jensen, A. G. 2017, *AJ*, 153, 217
- Cauley, P. W., Redfield, S., & Jensen, A. G. 2017, *AJ*, 153, 81
- Cegla, H. M., Lovis, C., Bourrier, V., et al. 2016, *A&A*, 588, 127
- Charbonneau, D., Brown, T. M., Noyes, R. W., & Gilliland, R. L. 2002, *ApJ*, 568, 377
- Chen, G., Pallé, E., Nortmann, L., et al. 2017, *A&A*, 600, L11
- Christie, D., Arras, P., & Li, Z.-Y. 2013, *ApJ*, 772, 144
- Collados, M., Lagg, A., Díaz Garcí A, J. J., et al. 2007, *ASPC 368, The Physics of Chromospheric Plasmas*, ed. P. Heinzel, I. Dorotovič, & R. J. Rutten (San Francisco, CA: ASP), 611
- Czesla, S., Klocová, T., Khalafinejad, S., Wolter, U., & Schmitt, J. H. M. M. 2015, *A&A*, 582, A51
- Deming, D., Wilkins, A., McCullough, P., et al. 2013, *ApJ*, 774, 95
- Dumusque, X., Boisse, I., & Santos, N. C. 2014, *ApJ*, 796, 132
- Ehrenreich, D., Bourrier, V., Wheatley, P. J., et al. 2015, *Nature*, 522, 459
- Ermolli, I., Criscuoli, S., Uitenbroek, H., et al. 2010, *A&A*, 523, 55
- Fares, R., Bourrier, V., Vidotto, A. A., et al. 2017, *MNRAS*, 471, 1246
- Gaudi, S., Stassun, K. G., Collins, K. A., et al. 2017, *Nature*, 546, 514
- Gondoin, P. 2008, *A&A*, 478, 883
- Gray, R. O., & Corbally, C. J. 1994, *AJ*, 107, 742
- Herrero, E., Ribas, I., Jordi, C., Morales, J. C., Perger, M., & Rosich, A. 2016, *A&A*, 586, A131
- Hestroffer, D., & Magnan, C. 1998, *A&A*, 333, 338
- Huang, C., Arras, P., Christie, D., & Li, Z.-Y. 2017, submitted to *ApJ*
- Jensen, A. G., Redfield, S., Endl, M., et al. 2011, *ApJ*, 743, 203
- Jensen, A. G., Redfield, S., & Endl, M., et al. 2012, *ApJ*, 751, 86
- Johns-Krull, C. M., Hawley, S. L., Basri, G., & Valenti, J. A. 1997, *ApJS*, 112, 221
- Judge, P. G., Kleint, L., & Sainz Dalda, A. 2015, *ApJ*, 814, 100
- Kahil, F., Riethmüller, T. L., & Solanki, S. K. 2017, *ApJS*, 229, 12
- Khalafinejad, S., von Essen, C., Hoeijmakers, H. J., et al. 2017, *A&A*, 598, A131
- Knutson, H. A., Charbonneau, D., Noyes, R. W., Brown, T. M., & Gilliland, R. L. 2007, *ApJ*, 655, 564
- Kreidberg, L., Bean, J. L., Désert, J.-M., et al. 2014, *Nature*, 505, 69
- Kreidberg, L., Line, M. R., Bean, J. L., et al. 2015, *ApJ*, 814, 66
- Kuckein, C., Collados, M., & Manso Sainz, R. 2015, *ApJ*, 799, 25
- Kuckein, C., Verma, M., Denker, C. 2016, *A&A*, 589, A84
- Louden, T., & Wheatley, P. J. 2015, *ApJL*, 814, L24
- Lund, M. B., Rodriguez, J. E., Zhou, G., et al. 2017, *AJ*, 154, 5
- Mandal, S., Chatterjee, S., & Banerjee, D. 2017, *ApJ*, 835, 158
- Martin, S. F. 1998, *Sol Phys*, 182, 107
- Meunier, N., Desort, M., & Lagrange, A.-M. 2010, *A&A*, 512, A39
- Morris, B. M., Hebb, L., Davenport, J. R. A., Rohn, G., & Hawley, S. L. 2017, *ApJ*, 846, 99
- Oklopčić, A., & Hirata, C. M. 2018, *ApJ*, 855, 11
- Pont, F., Sing, D. K., Gibson, N. P., et al. 2013, *MNRAS*, 432, 2917
- Rackham, B., Espinoza, N., Apai, D., et al. 2017, *ApJ*, 834, 151
- Rackham, B., Apai, D., & Giampapa, M. S. 2018, *ApJ*, 853, 122
- Redfield, S., Endl, M., Cochran, W. D., & Koesterke, L. 2008, *ApJ*, 673, L87
- Seager, S., & Sasselov, D. D. 2000, *ApJ*, 537, 916
- Shapiro, A. I., Solanki, S. K., Krivova, N. A., et al. 2014, *A&A*, 569, A38
- Sing, D. K., Pont, F., Aigrain, S., et al. 2011, *MNRAS*, 416, 1443
- Sing, D. K., Fortney, J. J., Nikolov, N., et al. 2016, *Nature*, 529, 59
- Snellen, I. A. G., Albrecht, S., de Mooij, E. J. W., & Le Poole, R. S. 2008, *A&A*, 487, 357
- Snellen, I. A. G., de Kok, R. J., de Mooij, E. J. W., & Albrecht, S. 2010, *Nature*, 465, 1049
- Snellen, I. A. G., Brandl, B., R., de Kok, R., J., et al. 2014, *Nature*, 509, 63
- Spake, J. J., Sing, D. K., Evans, T. M., et al. 2018, *Nature*, 557, 68
- Sütterlin, P. & Wiehr, E. 1998, *A&A*, 336, 367
- Title, A. M., Topka, K. P., Tarbell, T. D., et al. 1992, *ApJ*, 393, 782
- Turner, J. D., Christie, D., Arras, P., Johnson, R. E., & Schmidt, C. 2016, *MNRAS*, 458, 3880
- Unruh, Y. C., Solanki, S. K., & Fligge, M. 1999, *A&A*, 345, 635

- Vidal-Madjar, A., Lecavelier des Etangs, A., Désert, J.-M., et al. 2003, *Nature*, 422, 143
- Viticchié, B., Sánchez Almeida, J., Del Moro, D., & Berrilli, F. 2011, *A&A*, 526, A60
- von der Lühe, O. 1998, *NewAR*, 42, 493
- White, O. R., & Suemoto, Z. 1968, *SoPh*, 3, 523
- Wilson, P. A., Sing, D. K., Nikolov, N., et al. 2015, *MNRAS*, 450, 192
- Wytttenbach, A., Ehrenreich, D., Lovis, C., Udry, S., & Pepe, F. 2015, *A&A*, 577, A62
- Wytttenbach, A., Lovis, C., Ehrenreich, D., et al. 2017, *A&A*, 602, 36
- Xu, Y., Cao, W., Ding, M., et al. 2016, *ApJ*, 819, 89
- Yan, F., Fosbury, R. A. E., Petr-Gozens, M. G., Zhao, G., & Pallé, E. 2015, *A&A*, 574, 94
- Yan, F., Pallé, E., Fosbury, R. A. E., Petr-Gozens, M. G., & Henning, Th. 2017, *A&A*, 603, 73
- Zellem, R. T., Swain, M. R., Roudier, G., et al. 2017, *ApJ*, 844, 27